

# The *ASCA* Medium Sensitivity Survey (the GIS Catalog Project): Source Counts and Evidence for Emerging Population of Hard Sources

Yoshihiro Ueda<sup>1</sup>, Tadayuki Takahashi<sup>1</sup>, Yoshitaka Ishisaki<sup>2</sup>, Takaya Ohashi<sup>2</sup>,  
and Kazuo Makishima<sup>3</sup>

## ABSTRACT

We present first results from the *ASCA* Medium Sensitivity Survey (AMSS; or the GIS catalog project). From the serendipitous fields amounting to 106 deg<sup>2</sup>, we determined the Log  $N$  - Log  $S$  relations in the 0.7–7 keV and 2–10 keV bands with the best statistical accuracy obtained so far, over the flux range from  $1 \times 10^{-11}$  to  $5 \times 10^{-14}$  and  $7 \times 10^{-14}$  erg s<sup>-1</sup> cm<sup>-2</sup>, respectively. When the sources detected in the 0.7–7 keV band are divided into two subsamples with higher and lower spectral hardness, the former exhibits a significantly steeper slope than the latter at fluxes below  $\sim 10^{-12}$  erg s<sup>-1</sup> cm<sup>-2</sup> (0.7–7 keV). The average spectrum of sources becomes continuously harder toward fainter fluxes, from a photon index of 2.1 in the 0.7–10 keV range at the flux of  $\sim 10^{-11}$  to 1.6 at  $\sim 10^{-13}$  erg s<sup>-1</sup> cm<sup>-2</sup> (0.7–7 keV). This is consistent with the comparison of source counts between the 2–10 keV and the 0.7–2 keV band, and solves the puzzle of their discrepancy reported previously. Our results demonstrate rapid emergence of hard X-ray sources with a decreasing flux from  $\sim 10^{-12}$  to  $\sim 10^{-13}$  erg s<sup>-1</sup> cm<sup>-2</sup> (2–10 keV).

*Subject headings:* cosmology: diffuse radiation — galaxies: active

## 1. Introduction

X-ray surveys are the most direct approach to reveal the nature of sources that contribute to the Cosmic X-ray Background (CXB or XRB; see Fabian and Barcons 1989 for review). The *ROSAT* satellite resolved 70–80% of the CXB in the 0.5–2 keV band into discrete sources, whose majority are Active Galactic Nuclei (AGNs) (e.g., Hasinger *et al.* 1998; Schmidt *et al.* 1998). Because of the technical difficulties, imaging sky surveys in the hard X-ray band (above 2 keV), where the bulk of the CXB emission arises, were not available until the launch of *ASCA* (Tanaka, Inoue, and Holt, 1993). Deep/medium surveys performed with *ASCA* (Ogasaka *et al.* 1998; Ueda *et al.* 1998; 1999) and *BeppoSAX* (Fiore *et al.* 1999) have resolved a significant fraction (25–35%) of the CXB above 2 keV. The results indicate emergence of faint, hard X-ray sources that could be responsible in producing the CXB spectrum, which is harder than that of nearby type-I AGNs.

These surveys, though novel, are limited in sky coverage. As a result, the sample size of detected sources is not sufficient to obtain a self-consistent picture about the evolution of the sources over the wide fluxes, from  $\sim 10^{-11}$  erg s<sup>-1</sup> cm<sup>-2</sup> (2–10 keV) which is the sensitivity limit of *HEAO1* A2 (Piccinotti *et al.* 1982), down to  $\sim 10^{-13}$  erg s<sup>-1</sup> cm<sup>-2</sup> (2–10 keV), that of *ASCA* (e.g., Ueda *et al.* 1999). In particular, the

---

<sup>1</sup>Institute of Space and Astronautical Science, Yoshinodai 3-1-1, Sagamihara, Kanagawa 229-8510, Japan

<sup>2</sup>Department of Physics, Tokyo Metropolitan University, Hachioji, Tokyo 192-0397, Japan

<sup>3</sup>Department of Physics, University of Tokyo, Bunkyo-ku, Tokyo 113, Japan

broad band properties of sources at these fluxes are somewhat puzzling according to previous studies. The source counts in the soft band (0.3–3.5 keV) obtained by *Einstein* Extended Medium Sensitivity Survey (EMSS; Gioia *et al.* 1990) is about 2 times smaller than that in the hard band (2–10 keV) obtained by the *Ginga* fluctuation analysis (Hayashida, Inoue, & Kii 1990; Butcher *et al.* 1997) when we assume a power-law photon index of 1.7. This may imply presence of many hard sources at the flux level of  $\sim 10^{-12}$  erg s $^{-1}$  cm $^{-2}$  (2–10 keV). Such evidence is not seen, however, in the spectrum of the fluctuation observed by *Ginga*, which shows a photon index of  $1.8 \pm 0.1$  in the 2–10 keV range (Butcher *et al.* 1997).

To complement these shortcomings of deep surveys, we have been working on the project called the “*ASCA* Medium Sensitivity Survey (AMSS)”, or the GIS catalog project (Ishisaki *et al.* 1995; Ueda *et al.* 1997; Takahashi *et al.* 1998). In the project, we utilize the GIS data from the fields that have become publicly available to search for serendipitous sources. The large field of view and the low-background characteristics make the GIS instrument ideal for this purpose (Ohashi *et al.* 1996; Makishima *et al.* 1996). In this letter, we present the first results obtained from the latest version of the GIS catalog, in which the data taken from May 1993 through December 1996 are analyzed. The source list and detailed description of the catalog will be presented in a separate paper. From the serendipitous fields amounting to 106 deg $^2$ , we derived the Log  $N$  - Log  $S$  relations in the 0.7–7 keV and 2–10 keV bands with the best statistical accuracy obtained so far, over the wide flux range of more than 2 decades. The AMSS sample, currently the largest sample in the 0.7–10 keV range, leads us to the best understanding of the statistical properties of sources that produce about 30% of the CXB.

## 2. Results

### 2.1. Field Selection and Data Used in the Analysis

The first *ASCA* GIS source catalog (Ueda *et al.* 1999, in preparation) contains 1345 sources, including “target sources” at which the observation is aimed, detected from 369 fields observed from 1993 May to 1996 December. The analysis method for source surveys is basically the same as applied for the *ASCA* LSS (Ueda *et al.* 1998; 1999) except that the SIS data are not used in the AMSS. In the procedure we took into account the complicated responses of the XRT and the detectors. The analysis procedure consists of two steps: **I. source detection** and **II. flux calculation**. In step I, raw images are cross-correlated (smoothed) with the position dependent PSF of the XRT and the GIS and source candidates are searched in the smoothed image. In step II, we perform a 2-dimensional maximum-likelihood fitting to the raw image with a model that consists of the background and source peaks found in step I, including that of a target source. Multiple observations of the same or overlapped fields are combined in the analysis. The following selection criteria are applied for the catalog: (1) the Galactic latitude  $|b|$  is higher than 10°, (2) the time-averaged count rate is less than 0.8 c s $^{-1}$  per sensor, (3) the exposure is longer than 5000 sec, and (4) the 2-dimensional fit in step II is successful (reduced  $\chi^2 < 1.7$ ). We also excluded any fields for which we could not model the surface profile adequately, such as the fields of bright cluster of galaxies.

In this paper, to limit our interest on the study of extra-galactic sources, we further selected the fields of  $|b| > 20^\circ$ , excluding observations of nearby galaxies of large angular size, star forming regions, and supernova remnants. Finally, we discarded the target sources from the source list to construct a complete sample consisting of only serendipitous sources. The sample contains 714 sources (above 5  $\sigma$  detection), of which 696, 323, and 438 sources are detected in the 0.7–7 keV (total), 2–10 keV (hard), and 0.7–2 keV (soft) band, respectively. The number of sources detected both in the total and hard bands, total and soft bands,

and hard and soft bands are 320, 423, and 266, respectively, and 266 sources are detected in all the survey bands. The total sky area covered amounts to  $106 \text{ deg}^{-2}$  and the sensitivity limits are  $5 \times 10^{-14}$ ,  $7 \times 10^{-14}$ , and  $2.6 \times 10^{-14} \text{ erg s}^{-1} \text{ cm}^{-2}$  for the 0.7–7 keV, 2–10 keV, and 0.7–2 keV survey band, respectively. For each field, we corrected the count rates for the Galactic absorption, whose column density is estimated from H I observations (Dickey & Lockman 1990). The LSS sources (Ueda *et al.* 1999) are not included in the sample, whereas most of the GIS data of the deep surveys are included there.

## 2.2. The Source Spectra

Figure 1 shows the correlation between the 0.7–7 keV flux and the hardness ratio in the 0.7–10 keV range,  $HR1$ , defined as  $(H - S)/(H + S)$ , where  $H$  and  $S$  represent the count rate within radius of  $5'.9$  around the source (corrected for vignetting, see Ueda *et al.* 1999) in the 2–10 keV and 0.7–2 keV bands, respectively. Due to the limited photon statistics, however, these spectral information of individual sources is subject to a large statistical error, typically by 0.03, 0.1, and 0.2 ( $1\sigma$ ) at fluxes of  $10^{-11}$ ,  $10^{-12}$ , and  $10^{-13} \text{ erg s}^{-1} \text{ cm}^{-2}$ , respectively. Hence, to study the average properties of the source spectra, we calculated the average value of  $HR1$  (weighting with their errors) in several flux ranges from sources detected in the total band. The results are plotted in Figure 1 with crosses. Since the sensitivity is given in count rate rather than in flux, we sort sources by count rate (not by flux), to avoid to introduce any selection effects that very hard (or soft) sources are difficult to detect at the flux close to the sensitivity limit of each observation. The dashed curves in Figure 1 show conditions that give the same count rate, and sources located in the regions between the two curves are used for calculation of average hardness ratio. It is clear from Figure 1 that the average spectrum becomes harder with a decreasing flux. The corresponding photon index (assuming a power law over the 0.7–10 keV band with no absorption) changes from 2.1 at the flux of  $\sim 10^{-11} \text{ erg s}^{-1} \text{ cm}^{-2}$  to 1.6 at  $\sim 10^{-13} \text{ erg s}^{-1} \text{ cm}^{-2}$  (0.7–7 keV).

## 2.3. Log $N$ - Log $S$ Relation

Using the sample, we derived the Log  $N$  - Log  $S$  relation independently in the three survey bands, 0.7–7 keV, 2–10 keV, and 0.7–2 keV, in the following manner. For each field, we calculated the observed area as a function of count rate,  $\Omega(S)$ , following the same procedure described in Ueda *et al.* (1999). In this process, we estimate the significance of detection expected for the given flux at every positions, utilizing the fitting model used in step II of the source finding procedure and taking into account the presence of the target source. In calculation of  $\Omega(S)$  we excluded the regions where the spill of the PSF from the target source is higher than 50% of the background, and did not count any sources detected within the excluded region. Then, after summing up from all the selected fields  $\Omega(S)$ , and  $N(S)$ , the number of sources in flux bin of  $dS$ , we calculated the “observed” Log  $N$  - Log  $S$  relation in the differential form by dividing  $N(S)$  by  $\Omega(S)$ .

To evaluate possible systematic errors in the observed Log  $N$  - Log  $S$  relations, we next performed a large number of Monte Carlo simulations with roughly the same exposure distribution as the real data: we created 1400 simulated image data, consisting of 400 pointings with an exposure of 20 ksec, 300 with 30 ksec, 500 with 40 ksec, 50 with 70 ksec, and 50 with 90 ksec. The Log  $N$  - Log  $S$  relation input to the simulations is taken to be the same as the one we derived from the AMSS. We then applied the same analysis procedure for these simulated data as for the real data, and compared the derived parameters with the input

parameters. We found an excess of the output source counts relative to the input ones, which is about 10% (20%) at  $S = 2 \times 10^{-13}$  ( $8 \times 10^{-14}$ )  $\text{erg s}^{-1} \text{cm}^{-2}$  and 20% (40%) at  $S = 7 \times 10^{-14}$  ( $3 \times 10^{-14}$ )  $\text{erg s}^{-1} \text{cm}^{-2}$  in the total (soft) band, while such deviation is negligible in the hard band. The deviation and its energy dependence are also seen in the case of the LSS (Ueda *et al.* 1999) and can be explained by the effect of the source confusion, because the positional resolution of the GIS becomes worse toward lower energies. Thus, we corrected the observed differential  $\text{Log } N - \text{Log } S$  relation for this effect with a multiplicative factor  $f$ , derived by the simulation, which has a form of  $f = 1/[\Delta \times (\log S - \log S_0)/(\log S_1 - \log S_0) + 1]$  for  $S < S_0$ , and  $f = 1$  for  $S > S_0$ , where  $\Delta = 0.2$  (0.4),  $S_0 = 5.9 \times 10^{-13}$  ( $2.2 \times 10^{-13}$ ), and  $S_1 = 7.4 \times 10^{-14}$  ( $2.7 \times 10^{-14}$ ), for the total (soft) band survey, respectively. These simulated data are also used to evaluate the systematic error due to the source confusion in determination of  $HR1$ : the amount of the bias is estimated to be  $-0.03$  at  $10^{-13} \text{ erg s}^{-1} \text{ cm}^{-2}$  (0.7–7 keV) and is negligibly small in brighter flux level. This bias has been taken into account in deriving the average hardness ratio in Figure 1.

Since we impose the maximum count rate in the field-selection criteria, very bright sources are intentionally excluded in our sample: this means there is an upper flux limit above which the sample becomes incomplete. The maximum count rate, 0.8 c/s/sensor including the background and the target sources, indicates the upper flux limit is higher than  $(1 \sim 1.5) \times 10^{-11} \text{ erg s}^{-1} \text{ cm}^{-2}$  (2–10 keV) for most of the fields, although it depends both on the spectrum and the brightness of the target source. In integrating the differential  $\text{Log } N - \text{Log } S$  relations, we set the upper flux limits at  $10^{-11} \text{ erg s}^{-1} \text{ cm}^{-2}$  for the 0.7–7 keV and 2–10 keV surveys, and  $5 \times 10^{-12} \text{ erg s}^{-1} \text{ cm}^{-2}$  for the 0.7–2 keV survey, and used previous results by *HEAO1 A2* (Piccinotti *et al.* 1982) as integral constants at the bright flux ends assuming a photon index of 1.7. The uncertainty in the completeness close to these limits does not affect our discussion below, which are made mainly based on the fluxes fainter than  $10^{-12} \text{ erg s}^{-1} \text{ cm}^{-2}$  (0.7–7 keV and 2–10 keV).

The large sample size enables us to derive  $\text{Log } N - \text{Log } S$  relations separately for sources with different spectra. In practice, considering the large statistical error in the hardness ratio for an individual source, we divide the sample into two, the “soft source sample”, consisting of sources with  $HR1$  smaller than  $-0.028$ , which corresponds to a photon index larger than 1.7, and the “hard source sample”, with a photon index smaller than 1.7. In the conversion from count rate into flux, we assumed a photon index of 1.6 (1.6) for the hard source sample and 1.9 (1.6) for the soft source sample in the 0.7–7 keV (2–10 keV) survey. These photon indices come from the average spectrum of each sample after correcting for biases of purely statistical origin, based on the simulation.

Figure 2 shows the integral  $\text{Log } N - \text{Log } S$  relations in the 0.7–7 keV survey band for the soft source sample (red curve), the hard source sample (blue curve), and the sum (black curve). The figure clearly demonstrates that sources with hard energy spectra in the 0.7–10 keV range are rapidly increasing with decreasing fluxes, compared with softer sources. The ratio of the hard source sample (with a photon index of less than 1.7) to the soft source sample changes from about 20% at the flux of  $10^{-12} \text{ erg s}^{-1} \text{ cm}^{-2}$  (0.7–7 keV) to about 50% at  $10^{-13} \text{ erg s}^{-1} \text{ cm}^{-2}$ . We confirmed by the simulations that any statistical biases does not produce such dramatic change as a function of flux. For the 2–10 keV survey, we show the sum of the soft and hard source samples in Figure 3 (black curve).

### 3. Discussion

First, for confirmation, we compared the  $\text{Log } N - \text{Log } S$  relation in the 0.7–2 keV band with the results by *ROSAT* in almost the same band (0.5–2 keV) (Hasinger 1998 and references therein). We found a good

agreement within the statistical error at  $S > 1 \times 10^{-13} \text{ erg s}^{-1} \text{ cm}^{-2}$  (0.7–2 keV) between the two, whereas we see a slight excess of the *ASCA* source counts by about 10–20% at  $S = 3 \times 10^{-14} \sim 1 \times 10^{-13} \text{ erg s}^{-1} \text{ cm}^{-2}$  (0.7–2 keV), which was also reported from the LSS (Ueda *et al.* 1999). Using the AMSS data, we found that these excess can be explained by contribution of hard sources that have an (apparent) photon index less than 1.7 in the 0.7–10 keV range, whose number density increases more rapidly than that of softer sources toward fainter fluxes in the 0.7–2 keV band. Thus, as is discussed in Ueda *et al.* (1999), it is plausible that the difference between the *ASCA* and *ROSAT* results can be accounted for by the presence of hard (or absorbed) sources, which are more easily detectable by *ASCA* than by *ROSAT*, due to their difference of energy dependence of the effective area even within the similar energy band.

The present results of the Log  $N$  - Log  $S$  relations in the three survey bands are all consistent with the LSS results (Ueda *et al.* 1999) within the statistical errors. The 2–10 keV source counts is also consistent with that by Cagnoni, Della Ceca, & Maccacaro (1998), who utilized the GIS2 data from about one fifth of the data set analyzed here, and with the fluctuation analysis of the *ASCA* SIS data by Gendreau, Barcons & Fabian (1998). In Figure 3, we show the constraints from the fluctuation analysis by *Ginga* (Butcher *et al.* 1997). As noticed, below the flux of  $10^{-12} \text{ erg s}^{-1} \text{ cm}^{-2}$  (2–10 keV), our direct source counts gives somewhat lower values than *Ginga*, although it is barely consistent within the 90% statistical errors.

The increasing fraction of hard sources toward fainter fluxes seen in Figure 2 accounts for the evolution of the average source spectra shown in Figure 1. The spectral evolution is also consistent with the comparison of the source counts between the hard and the soft band. In Figure 3, we compare the source counts in the hard band with that in the soft band, both obtained from the AMSS. In the figure, the 0.7–2 keV fluxes are converted into the 2–10 keV fluxes assuming the two photon indices (1.6 and 1.9). As is clearly seen, the source counts in the hard band survey increases more rapidly than that in the soft band survey toward the sensitivity limit. As a result, the hard band source counts at  $S \sim 10^{-13} \text{ erg s}^{-1} \text{ cm}^{-2}$  (2–10 keV) matches the soft band one when we assume a photon index of 1.6, whereas at brighter level of  $S = 4 \times 10^{-13} \sim 10^{-12} \text{ erg s}^{-1} \text{ cm}^{-2}$  (2–10 keV), we have to use a photon index of about 1.9 to make them match. These indices, which should represent average source spectra at each flux level, well coincide with those directly derived from Figure 1. It is also interesting that the slope of the Log  $N$  - Log  $S$  relation in the hard- and soft-source sample in the total band survey (Figure 2) is similar to that of the Log  $N$  - Log  $S$  relation in the hard- and soft-band survey (Figure 3), respectively, at the flux range of one decade above the sensitivity limit. This is expected if we roughly consider that the sources in the hard (soft) source sample correspond to those detected in the hard (soft) survey.

As discussed above, all the present results from the AMSS are perfectly consistent with one another. Consequently, the derived Log  $N$  - Log  $S$  relations covering the 0.7–10 keV range, determined by direct source counts, has now solved the puzzle of discrepancy of the source counts between the soft (EMSS) and the hard band (*Ginga* and *HEAO1*). They are now reconciled by the two facts: (1) the source counts in the hard band obtained by the AMSS is smaller than the best-fit value of the *Ginga* results at  $S = 4 \times 10^{-13} \sim 1 \times 10^{-12} \text{ erg s}^{-1} \text{ cm}^{-2}$  (2–10 keV) and (2) that in the soft band, which is consistent with the recent *ROSAT* surveys such as RIXOS (Mason *et al.* 1999), gives larger source counts by  $\sim 30\%$  than the EMSS results that include Galactic objects. As seen from Figure 1, the average spectrum of sources at  $S = 3 \times 10^{-13} \sim 3 \times 10^{-12} \text{ erg s}^{-1} \text{ cm}^{-2}$  (0.7–7 keV) has a photon index of 1.8–2.1 in the 0.7–10 keV range, indicating that the contribution of hard sources (such as heavily absorbed AGNs) is not significant yet at this flux level to reproduce the CXB spectrum. This fact can be connected with the “soft” spectrum of the fluctuation observed with *Ginga*, which shows a photon index of  $1.8 \pm 0.1$  in the 2–10 keV range (Butcher *et al.* 1997).

The emerging population of hard sources seen in Figure 2 can be understood by increasing contribution of absorbed AGNs, which should become more significant toward fainter flux level due to the K-correction effect as is discussed in the AGN synthesis model (Awaki *et al.* 1991; Comastri *et al.* 1995). In fact, optical identification of the *ASCA* LSS shows that most of the hard (or absorbed) sources are narrow-line or weak broad-line AGNs, and that their contribution is comparable to that of unabsorbed AGNs at the 2–10 keV flux of  $2 \times 10^{-13}$  erg s<sup>-1</sup> cm<sup>-2</sup> (Akiyama *et al.* 1999). Since the number of sources in the LSS sample is limited, the optical identification of the AMSS sample is crucial to reveal the evolution of each population, particularly that of absorbed AGNs, which are difficult to detect in the soft band. The integrated spectrum of sources with fluxes above  $\sim 10^{-13}$  erg s<sup>-1</sup> cm<sup>-2</sup> (2–10 keV) is not hard enough to completely account for the CXB spectrum. Our results thus predict that further hardening is necessary at fainter flux levels. This can be confirmed by future missions such as XMM and Chandra. On the other hand, at the brighter flux range,  $10^{-13} \sim 10^{-11}$  erg s<sup>-1</sup> cm<sup>-2</sup> (2–10 keV) where we need to cover large area to overcome the small surface number densities, the AMSS provides the best opportunity for statistical studies of X-ray sources in the universe.

We are grateful to Prof. H. Inoue for stimulating discussion. We thank members of the *ASCA* team for their support in satellite operation and data acquisition, and Dr. H. Kubo for the help in analysis.

## REFERENCES

- Akiyama, M., *et al.* 1999, ApJ, submitted
- Awaki, H., Koyama, K., Inoue, H., & Halpern, J.P. 1991, PASJ, 43, 195
- Butcher, J.A., *et al.* 1997, MNRAS, 291, 437
- Cagnoni, I., Della Ceca, R., & Maccacaro, T. 1998, ApJ, 493, 54
- Comastri, A., Setti, G., Zamorani, G., & Hasinger, G. 1995, A&A, 296, 1
- Dickey, J.M. & Lockman F.J. 1990, ARA&A, 28, 215
- Fabian, A.C., & Barcons, X. 1992, ARA&A, 30, 429
- Fiore, F., *et al.* 1999, MNRAS, 306, L55
- Gendreau, K.C., Barcons, X., & Fabian, A.C. 1998, MNRAS, 297, 41
- Gioia, I.M. *et al.* 1990, ApJS, 72, 567
- Hasinger, G. 1998, Astro. Nachr., 319, 37
- Hasinger, G., Burg, R., Giacconi, R., Schmidt, M., Trümper, J., & Zamorani, G. 1998, A&A, 329, 482
- Hayashida, K., Inoue, H., & Kii, T. 1990, in proc. of “Frontiers of X-ray Astronomy”, eds. Tanaka, Y. & Koyama, K., p653
- Ishisaki, Y., Takahashi, T., Kubo, H., Ueda, Y., Makishima, K., & the GIS Team 1995, the *ASCA* News No.3, NASA/Goddard Space Flight Center, p19
- Kondo, H. *et al.* 1982, in proc. of “Frontiers of X-ray Astronomy”, eds. Tanaka, Y. & Koyama, K., p655

- Makishima, K., *et al.* 1996, PASJ, 48, 171
- Mason, K.O., *et al.* 1999, MNRAS, in press
- Ogasaka, Y., *et al.* 1998, Astro. Nachr., 319, 43
- Ohashi, T., *et al.* 1996, PASJ, 48, 157
- Piccinotti, G., Mushotzky, R.F., Boldt, E.A., Marshall, F.E., Serlemitsos, P.J. & Shafer, R.A. 1982, ApJ, 253, 485
- Schmidt, M., Hasinger, G., Gunn, J., Schneider, D., Burg, R., Giacconi, R., Lehmann, I., Mackenty, J., Trümper, J., & Zamorani, G. 1998, A&A, 329, 495
- Takahashi, T., Ueda, Y., Ishisaki, Y., Ohashi, T., & Makishima, K. 1998, Astro. Nachr., 319, 91
- Tanaka, Y., Inoue, H., & Holt, S.S. 1994, PASJ, 46, L37
- Ueda, Y., Takahashi, T., Ishisaki, Y., Makishima, K. & 1997, in proc. of “All-Sky X-Ray Observations in the Next Decade”, eds. Matsuoka, M. & Kawai N., p55
- Ueda, Y., *et al.* 1998, Nature, 391, 866
- Ueda, Y., *et al.* 1999, ApJ, 518, 656

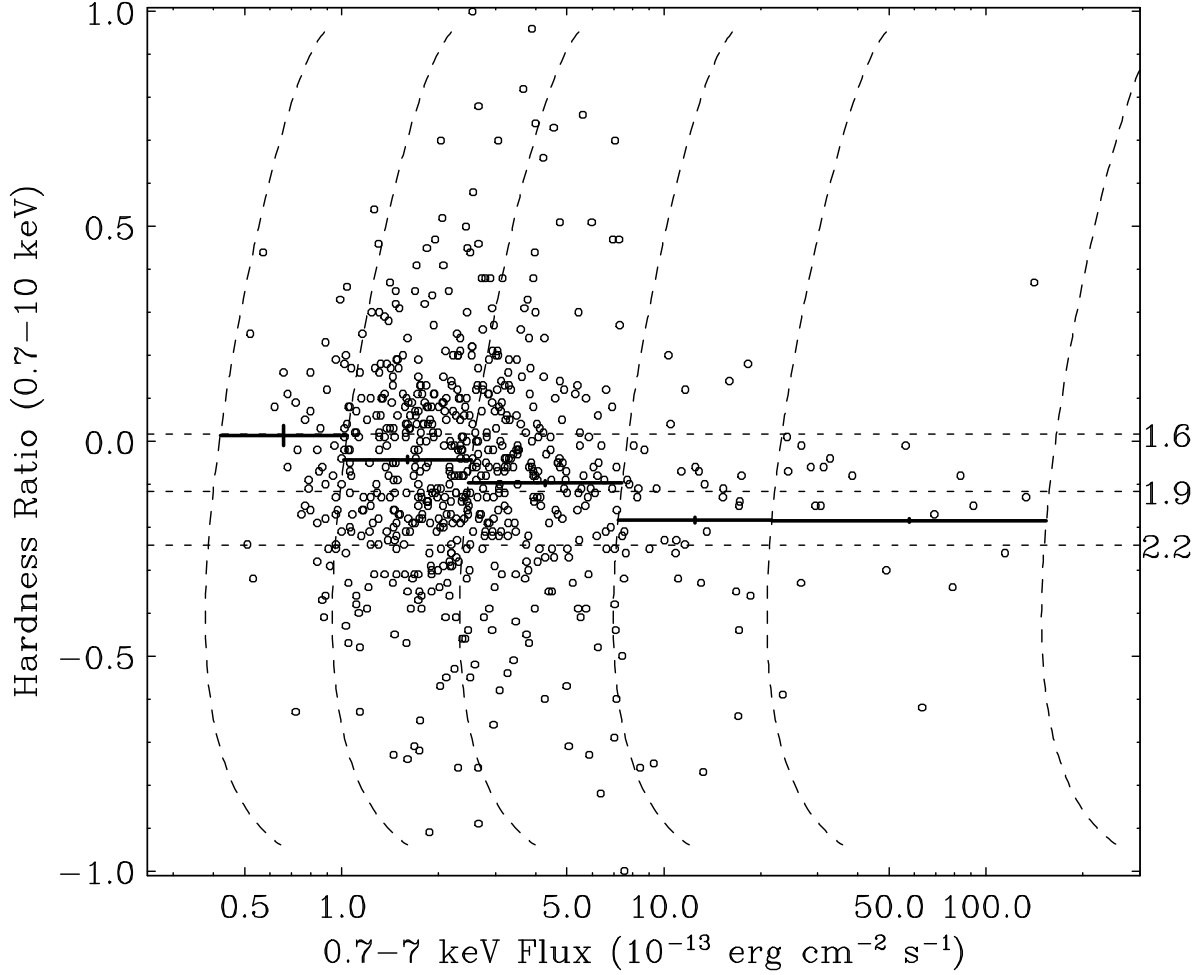


Fig. 1.— The correlation between the 0.7-7 keV flux and the hardness ratio ( $HR1$ ) between the 0.7-2 keV and 2-10 keV count rate for sources detected in the 0.7-7 keV survey in the AMSS sample. The count rate is converted into flux for each source based on the best-fit hardness assuming a power law spectrum and correcting for the Galactic absorption. The crosses show the average hardness ratios (with  $1\sigma$  errors in the mean value) in the flux bin separated by the the dashed curves, at which the count rate hence the sensitivity limit is constant. The dotted lines represent the hardness ratios corresponding to a photon index of 1.6, 1.9, and 2.2 assuming a power law spectrum. Absorption with  $N_{\text{H}} = 3 \times 10^{21}$   $\text{cm}^{-2}$  increases  $HR1$  by about 0.15.

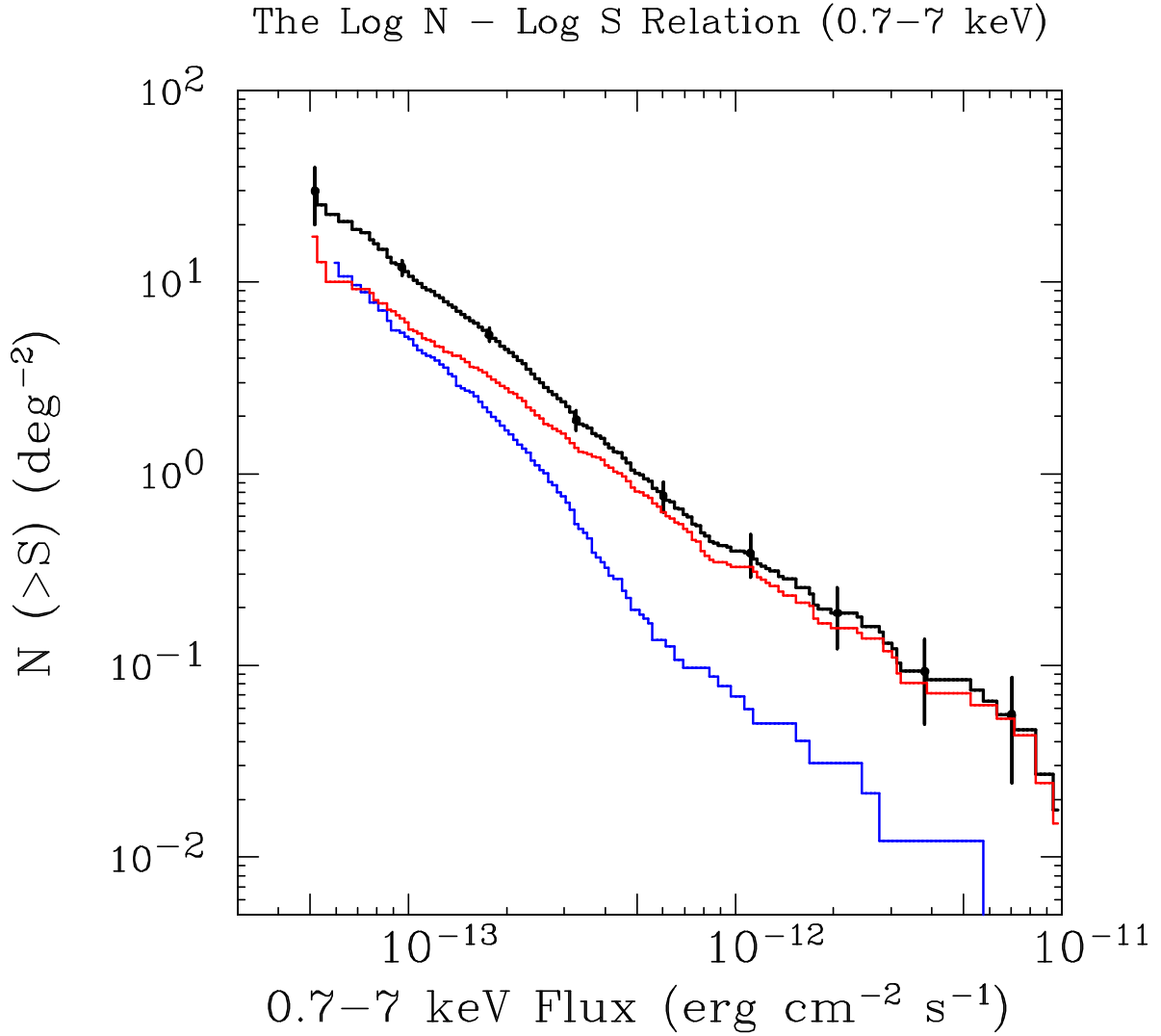


Fig. 2.— The integral Log  $N$  - Log  $S$  relations in the 0.7–7 keV survey band, derived from the AMSS sample. The blue curve represents the result for the hard source sample, consisting of sources with (apparent) photon indices less than 1.7 in the 0.7–10 keV range, the red curve represents that for the soft source sample (with indices larger than 1.7), and the black curve represents the sum. At several points, the 90% statistical errors in the source counts are plotted. A photon index of 1.6 and 1.9 is assumed in the count rate to flux conversion for the hard- and soft-source sample, respectively, with correction for the Galactic absorption.

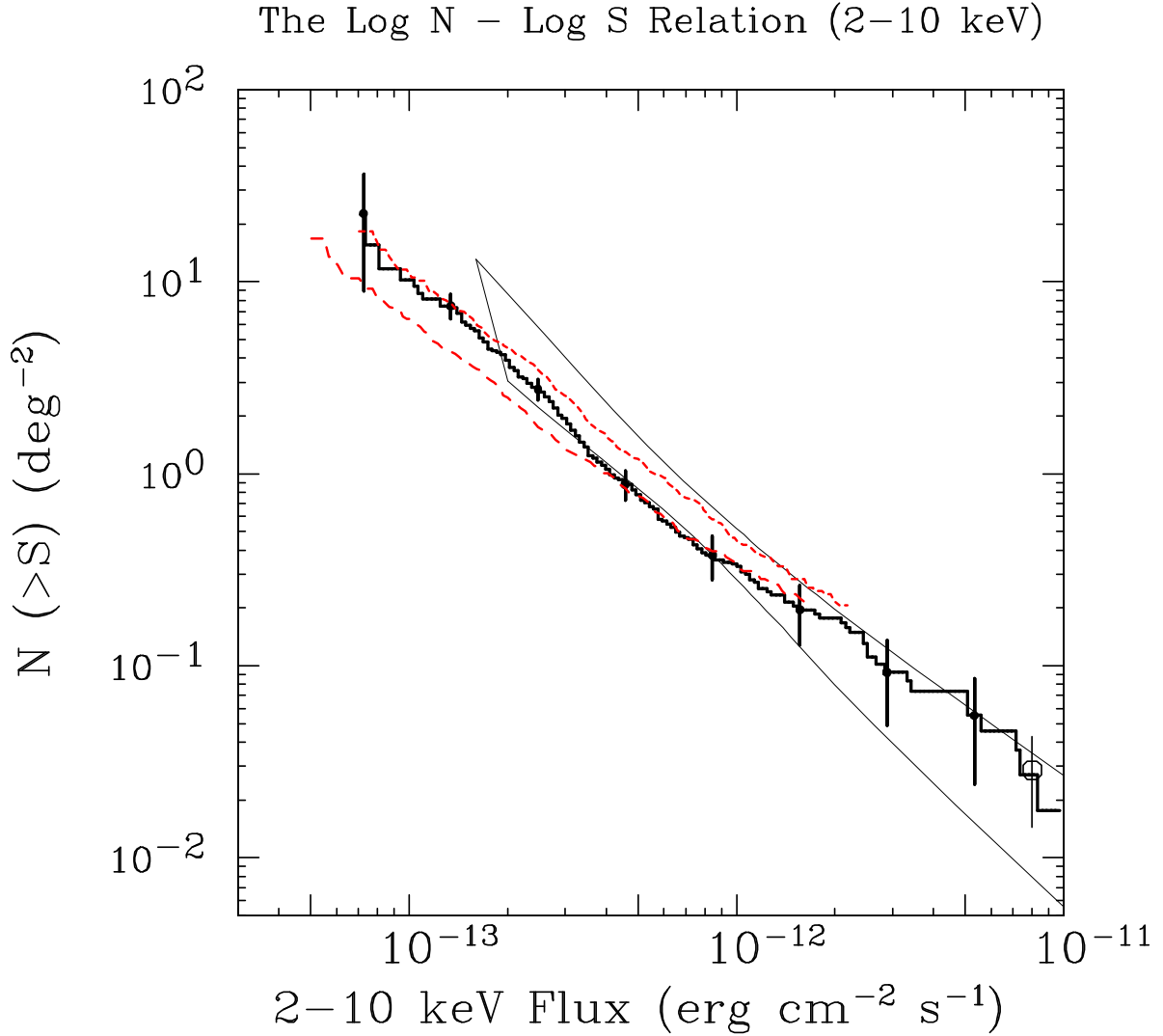


Fig. 3.— The integral Log  $N$  - Log  $S$  relations in the 2–10 keV band survey, derived from the AMSS sample. The elongated box represents the constraints by the *Ginga* fluctuation analysis (Butcher *et al.* 1997). The open circle corresponds to the source counts by *Ginga* survey (Kondo *et al.* 1991). The two dashed curves (red) are the Log  $N$  - Log  $S$  relations in the 0.7–2 keV band survey derived from the AMSS (this work), converted into the 2–10 keV flux assuming a power law with a photon index of 1.6 (short-dashed curve) and 1.9 (long-dashed curve).